

Complex structure reveals CcmM and CcmN form a heterotrimeric adaptor in β -carboxysome

Hui Sun | Ning Cui | Shu-Jing Han | Zhi-Peng Chen | Ling-Yun Xia |
Yuxing Chen | Yong-Liang Jiang | Cong-Zhao Zhou 

Hefei National Laboratory for Physical Sciences at the Microscale and School of Life Sciences, University of Science and Technology of China, Hefei, China

Correspondence

Cong-Zhao Zhou and Yong-Liang Jiang, Hefei National Laboratory for Physical Sciences at the Microscale and School of Life Sciences, University of Science and Technology of China, Hefei, Anhui 230027, China.

Email: zcz@ustc.edu.cn (C.-Z. Z.) and jyl@ustc.edu.cn (Y.-L. J.)

Funding information

Chinese Academy of Sciences, Grant/Award Numbers: XDA24020302, XDB37020301; National Natural Science Foundation of China, Grant/Award Numbers: 31621002, 31630001

Abstract

Carboxysome is an icosahedral self-assembled microcompartment that sequesters RuBisCO and carbonic anhydrases within a selectively permeable protein shell. The scaffolding proteins, CcmM, and CcmN were proposed to act as adaptors that crosslink the enzymatic core to shell facets. However, the details of interaction pattern remain unknown. Here we obtained a stable heterotrimeric complex of CcmM γ -carbonic anhydrase domain (termed CcmM^{NT}) and CcmN, with a 1:2 stoichiometry, which interacts with the shell proteins CcmO and CcmL in vitro. The 2.9 Å crystal structure of this heterotrimer revealed an asymmetric bundle composed of one CcmM^{NT} and two CcmN subunits, all of which adopt a triangular left-handed β -helical barrel structure. The central CcmN subunit packs against CcmM^{NT} and another CcmN subunit via a wall-to-edge or wall-to-wall pattern, respectively. Together with previous findings, we propose CcmM^{NT}-CcmN functions as an adaptor to facilitate the recruitment of shell proteins and the assembly of intact β -carboxysome.

KEYWORDS

adaptor, carboxysome assembly, CO₂-concentrating mechanism, crystal structure

1 | INTRODUCTION

Cyanobacteria and many other carbon-assimilating bacteria have developed a CO₂-concentrating mechanism (CCM), which significantly enhances the efficiency of CO₂-fixation by sequestered enzymes of RuBisCO.¹ The CCM is composed of a couple of carbon-uptake systems² and carboxysome, a large protein machinery that encapsulates RuBisCO^{3,4} and carbonic anhydrases (CA)⁵ in a selectively permeable protein shell.^{6,7} As a well investigated bacterial microcompartment (BMC), carboxysome self-assembles into a large icosahedral organelle of 100–400 nm in diameter from thousands of proteins.^{8–11}

Despite most components of carboxysome have been intensively studied from the structural point of view,^{12–22} it remains unknown on how the mature carboxysome assembles via sequential condensation and regular stacking of these components.

Based on the form of RuBisCO encapsulated, carboxysomes have been classified into two types: α and β . The α -carboxysomes possess Form-1A RuBisCO, whereas β -carboxysomes sequester plant-like Form-1B RuBisCO.²³ Both types of carboxysome share a similar structural organization, which contains an inner core of dense enzymatic cargo of RuBisCO and CA, encapsulated by the icosahedral shell composed of hexameric and pentameric proteins.¹⁰ However, distinct mechanisms were proposed for their assembly: the α -carboxysome co-assembles the shells concomitantly with the aggregation of cargo enzymes,^{11,24}

Y.-L.J. thanks the Youth Innovation Promotion Association of Chinese Academy of Sciences for their support.

whereas the β -carboxysome assembles in an inside-out manner initiating with the condensation of the inner core.^{11,25} Beyond the shell and cargo proteins, scaffolding proteins serve as adaptors that crosslink various components. In α -carboxysome, the scaffolding protein CsoS2, which is intrinsically disordered, functions as a multivalent interaction hub that condenses and recruits RuBisCO to the nascent carboxysome shell facets, ultimately enabling the intact carboxysome formation.^{26–29} In β -carboxysome, two conserved scaffolding proteins, CcmM, and CcmN were proposed to act in concert to bridge the shell and cargo proteins.^{30–34} The coding genes of CcmM and CcmN are located adjacently within the core *ccm* operon (Figure 1a); however, quantitative analysis of β -carboxysome proteins in cell lysates revealed a substantial quantity of CcmM, and non-detectable CcmN,^{30,33,35} indicating that CcmM is of much higher cellular abundance compared to CcmN.

The cyanobacteria encode a full-length CcmM containing an N-terminal γ -carbonic anhydrase-like domain (termed CcmM^{NT}) followed by three to five RuBisCO small subunit-like (SSUL) modules, in addition to a truncated version that consists of only the SSUL modules via alternative translation initiation.^{32,36,37} In *Synechococcus elongatus* PCC7942, the 58-kDa full-length CcmM was termed CcmM58, whereas the 35-kDa truncated version was termed CcmM35 (Figure 1b). It was found that the SSUL modules of CcmM bind close to the equatorial region of native L8S8 RuBisCO between two RbcL dimers, inducing the formation of RuBisCO condensates in β -carboxysome biogenesis.³⁸ Yeast two-hybrid analysis and pull-down experiments indicated that CcmM^{NT} interacts with CcmN to facilitate the association of inner cargo with the outer shell.^{31,34} In addition, CcmM was also found to interact with the shell proteins, including CcmK1/K2/K4/L.^{31,39} CcmM^{NT} from *Thermosynechococcus elongatus* BP-1, which represents the only known structure of γ -CA domain, adopts a left-

handed β -helix fold, with the γ -CA activity under the regulation of redox state via an essential disulfide bond.¹⁷

As shown in Figure 1b, CcmN has two regions of distinct function: an N-terminal domain harboring six bacterial hexapeptide repeats (Pfam00132) and a C-terminal encapsulation peptide (EP) of an amphipathic α -helix.^{34,40} Deficiency of the full-length CcmN or only the C-terminal EP in *S. elongatus* PCC7942 resulted in defect of carboxysome formation, suggesting an important role of CcmN, especially the C-terminal EP, in carboxysome assembly.^{25,34} Sequence analysis revealed that CcmN shows a 24% sequence identity with CcmM^{NT}, indicating they most likely share a similar fold. It was proposed that N-terminal domain of CcmN binds to CcmM^{NT}, whereas the EP anchors to CcmK2, probably as well as other shell proteins.^{34,39,41} In addition, the counterparts of CcmN C-terminal EP have also been found in the encapsulated proteins of other BMCs, indicating its universal role in BMC assembly.^{40,42,43} However, it remains unknown how CcmM and CcmN interact with each other, and further mediate the β -carboxysome assembly.

Here we obtained a stable complex of the heterotrimeric CcmM^{NT}-CcmN from *S. elongatus* PCC7942 and solved its crystal structure at 2.9 Å resolution. Biochemical assays and structural analysis demonstrated that the CcmM^{NT}-CcmN complex serves as an adaptor that bridges the inner core enzymes and the shell proteins of β -carboxysome.

2 | RESULTS

2.1 | Crystal structure of CcmM^{NT} in complex with CcmN

Overexpression of *S. elongatus* PCC7942 full-length CcmN in *Escherichia coli* yielded aggregates, even with an

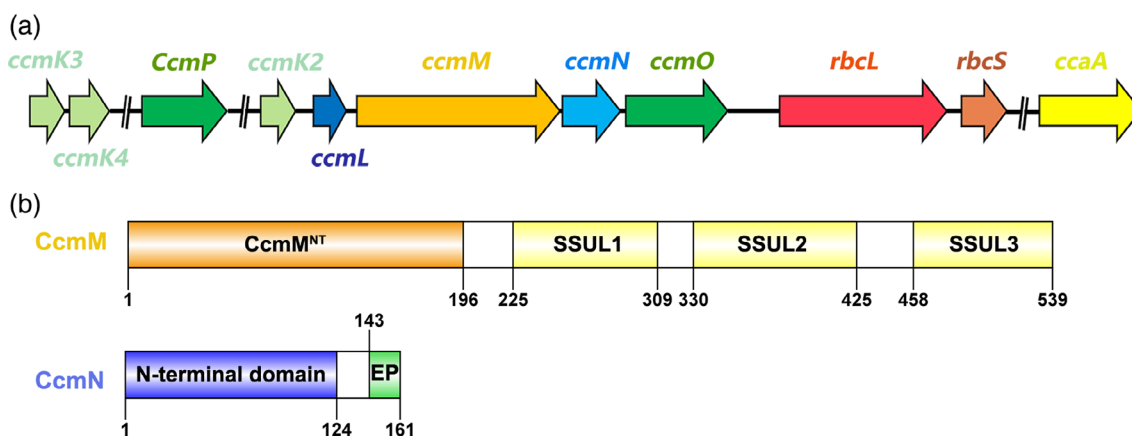


FIGURE 1 A scheme of CcmM and CcmN in *S. elongatus* PCC7942. (a) Genomic organization of carboxysome in *S. elongatus* PCC7942. The *ccmM* and *ccmN* genes are located in the same operon. (b) Domain organizations of CcmM and CcmN proteins

SUMO-tag fused at the N-terminus; however co-expression the SUMO-CcmN with CcmM^{NT} that covers residues Met1-Ser209 of CcmM (Table S1) eventually enabled us to purify a stable homogeneous complex of SUMO-CcmN with CcmM^{NT} (Figure S1). This complex has a molecular weight of ~84 kDa, as estimated by size-exclusion chromatography coupled with multi-angle static light scattering (SEC-MALS) (Figure S2A), which is comparable to the theoretical mass of a heterotrimeric complex composed of one CcmM^{NT} and two SUMO-CcmN subunits.

To further figure out the interactions between CcmM^{NT} and CcmN, we solved the 2.9 Å crystal structure of CcmM^{NT}-CcmN complex in space group $P2_12_12_1$ by molecular replacement (Figure 2a). Of note, only residues Met1-Pro118 of CcmN could be traced in the structure, leaving the N-terminal SUMO-tag and the C-terminal EP segment invisible in the electron density map. In the refined structure, each asymmetric unit contains two CcmM^{NT} molecules and four CcmN molecules, with a 1:2 stoichiometry. The CcmM^{NT} subunit adopts a

core structure of seven-turn left-handed β -helical barrel of ~37 Å in height, with helix α A capped on one opening and helix α B sticking to one wall of the β -barrel (Figure 2a). The overall structure of CcmM^{NT} subunit (covering residues from Ala16 to Pro184) closely resembles the structure of the inactive-form CcmM193 (residues 1–193 of CcmM, PDB: 3KWD) from *T. elongatus* BP-1,¹⁷ with a root-mean-square deviation (RMSD) of 0.585 Å over 145 C α atoms (Figure 2b). In contrast, the corresponding segments, including the N-terminal β 1, β 1– β 2 loop and C-terminal helix α C which were proven to be necessary for the γ -CA activity in the active-form *T. elongatus* CcmM209 (residues 1–209 of CcmM, PDB: 3KWC), are disordered in our recombinant CcmM^{NT} of 209 residues (Figure 2b). Moreover, the disulfide-bonded residues Cys194 in α B and Cys200 in α C, which are critical for γ -CA activity of *T. elongatus* CcmM209, are absent in CcmM^{NT} (Figure S3A). In fact, it was previously reported that CcmM^{NT} is a degenerated CA, despite it possesses the central catalytic residues His73, His100, and His105.⁴⁴

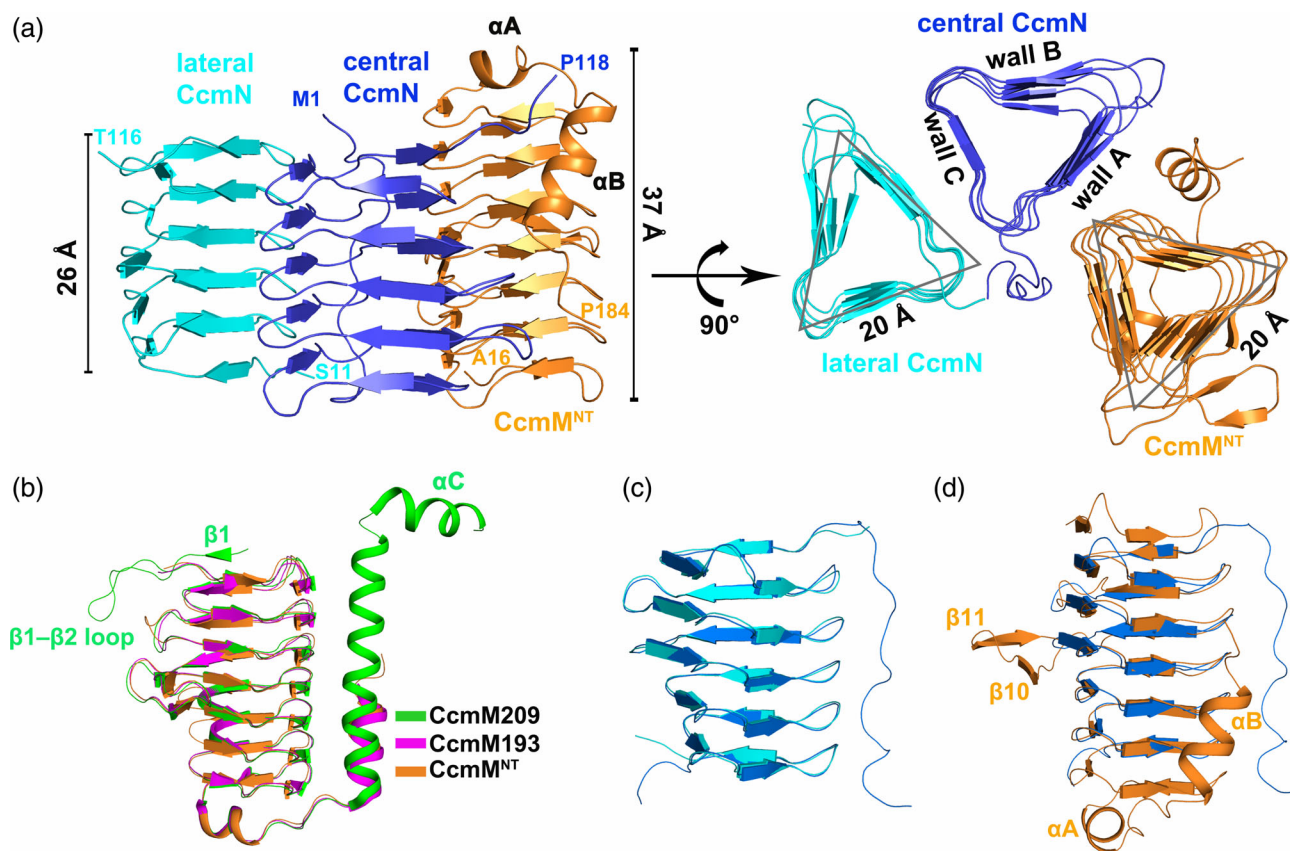


FIGURE 2 The complex structure of CcmM^{NT}-CcmN. (a) Cartoon representation of the overall structure of CcmM^{NT}-CcmN, shown in the top and side views. The CcmM^{NT} subunit is colored in orange, whereas the two CcmN subunits are shown as blue and cyan, respectively. The traced residues at the most N- and C-termini are marked. (b) Superposition of CcmM^{NT} (orange) against *T. elongatus* BP-1 CcmM209 (3KWC; green) and CcmM193 (3KWD; magenta). The additional segments of β 1, β 1– β 2 loop and helix α C from CcmM209 are labeled. (c) Superposition of two CcmN subunits in the heterotrimeric complex of CcmM^{NT}-CcmN. The central CcmN (blue) has an extension of a 10-residue N-terminal segment, compared to the lateral CcmN (cyan). (d) Superposition of the central CcmN (blue) onto CcmM^{NT} (orange)

The two CcmN subunits also adopt a left-handed β -helical barrel structure similar to CcmM^{NT}, but with a ~ 26 -Å high core structure of only five turns. Each turn of the β -helix consists of three short β -strands, forming an equilateral triangle of 20 Å in side length from the top view. The triangular CcmN β -barrel has three flat exposed walls (termed walls A–C, respectively), in which walls A and C are generally hydrophobic, and wall B is hydrophilic. Notably, beyond the core β -helix structure, the central CcmN subunit possesses an additional 10-residue N-terminal segment that folds against the core structure and stretches across one edge of the β -barrel (Figure 2c), compared to the lateral CcmN subunit. In addition, the overall structure of CcmN is similar to that of CcmM^{NT}, with an RMSD of 0.735 Å over 83 C α atoms of the β -helical barrel (Figure 2d). However, CcmM^{NT} has two more turns of β -helix, two extra α -helices at the C-terminus, in addition to a 14-residue insertion of two protruded β -strands (β 10 and β 11) and connecting loops, compared to CcmN.

2.2 | The interactions between CcmM^{NT} and CcmN

In the CcmM^{NT}-CcmN complex, the central CcmN subunit interacts with both CcmM^{NT} and the lateral CcmN subunit via two different interfaces. The wall C of central CcmN subunit packs against the wall A of lateral CcmN subunit, forming an interface of $\sim 1,000$ Å², mainly mediated by hydrophobic interactions, in addition to a hydrogen bond Arg59-Gly68 (Figure 3a). In contrast, one edge of the triangular CcmM^{NT} β -barrel interacts with the wall A of central CcmN subunit (Figure 3b), yielding an interface area of $\sim 1,000$ Å². In addition to extensive hydrophobic interactions, several polar interactions, including the hydrogen bonds Arg119-Gly74 and Arg119-Thr94, also contribute to stabilizing the interface. Notably, the N-terminal residue Glu7 of central CcmN subunit forms a hydrogen bond with His73 of CcmM^{NT} to further strengthen the interface. Sequence analysis showed that most residues at the interface from both CcmN and CcmM are relatively conserved (Figure S3), indicating a similar interaction pattern among the homologs.

The individual CcmM^{NT} forms a stable trimer in solution, as confirmed by the SEC–MALS analysis (Figure S2B). Based on the structure of *T. elongatus* CcmM209 (PDB: 3KWC)¹⁷ which shares a 67% sequence identity, we built a model of *S. elongatus* PCC7942 CcmM^{NT} trimer, with one edge and the C-terminal α B helix of one subunit packing along one wall of the symmetric subunit. Notably, compared to the simulated CcmM^{NT} trimer with an interface of ~ 800 Å², the central

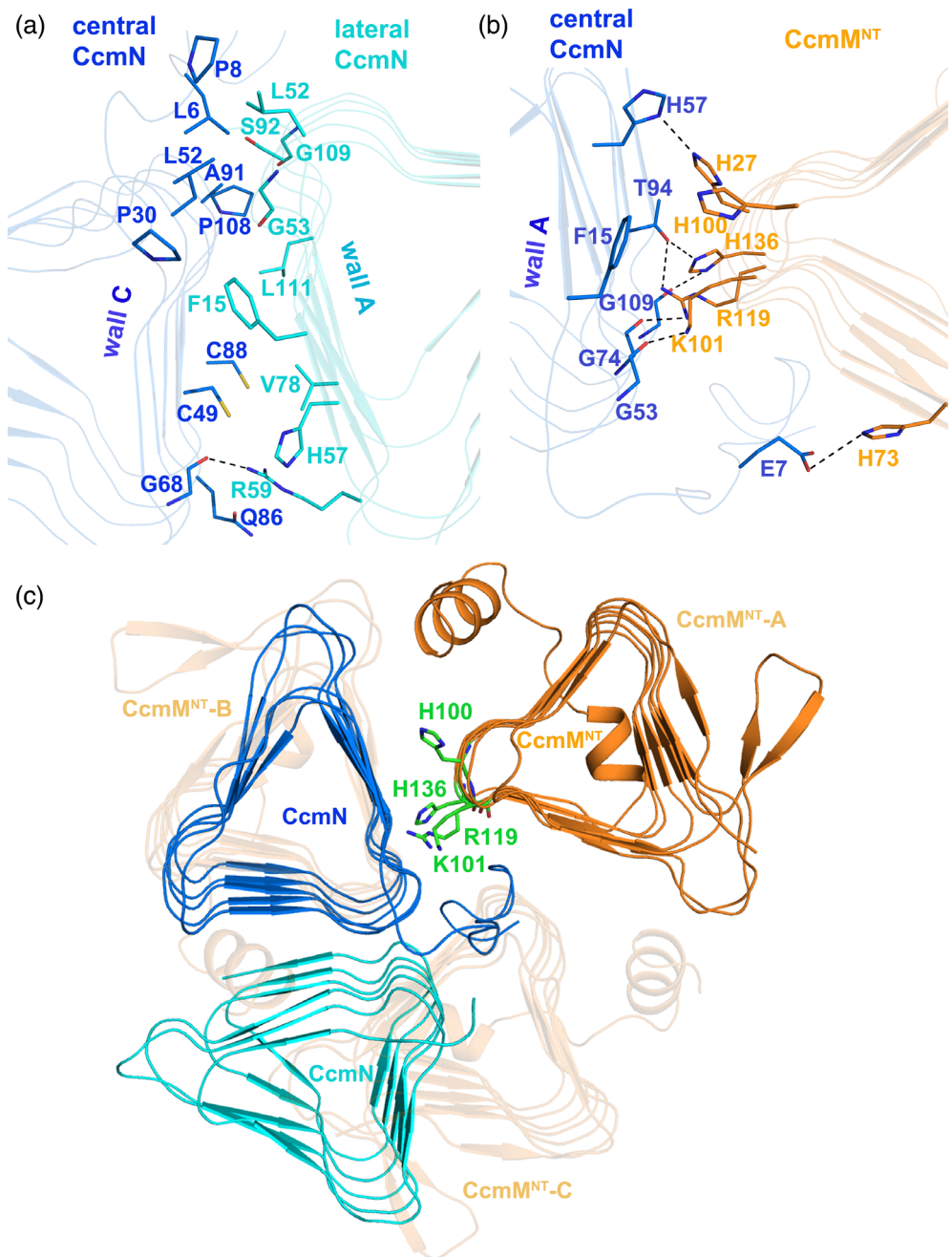
CcmN subunit binds to the same face of CcmM^{NT} with a larger interface area of $\sim 1,000$ Å². Thus we speculated that CcmM^{NT} subunits can bind to either CcmM^{NT} or CcmN subunits in a similar wall-to-edge manner, to form either CcmM^{NT} homotrimers or CcmM^{NT}-CcmN heterotrimers. Moreover, the abundant hydrophobic residues exposed on the walls A and C of CcmN enable two CcmN subunits to pack against each other in a wall-to-wall manner (Figure 3c). The surface-exposed hydrophobic walls of CcmN also explain why the individual CcmN is prone to forming large aggregates.

2.3 | The CcmM^{NT}-CcmN complex functions as an adaptor inside of β -carboxysome shell via interacting with CcmO and CcmL

Previous findings suggested that CcmN interacts with the hexameric shell protein CcmK2, and other shell proteins, mediating the association of cargo proteins with the shell.^{34,39,41} Moreover, CcmM was found to interact with several shell proteins probably via CcmM^{NT}.^{31,32,39} To further identify the binding partners of CcmM^{NT}-CcmN complex, we used *E. coli* to systematically co-express the His-tagged CcmM^{NT}-CcmN complex with the FLAG-tagged shell proteins, including the hexameric CcmK2, CcmK3, and CcmK4, the trimeric CcmP and CcmO, in addition to the vertex protein of pentameric CcmL (Table S1). Afterwards, we checked whether these shell proteins could interact with the CcmM^{NT}-CcmN complex by nickel-NTA affinity purification. The results showed that a large amount of CcmO and CcmL proteins could be pulled down, whereas only very little amount of CcmK2 was detected by denaturing gel electrophoresis (SDS-PAGE) (Figure 4a). In contrast, the other shell proteins were not detectable at all (Figure 4a).

To further test whether the C-terminal EP of CcmN contributes to the interaction with CcmO or CcmL, we constructed a truncated version of His-tagged CcmN lacking the C-terminal 18-residue EP (termed CcmN Δ EP), and co-purified the CcmM^{NT}-CcmN Δ EP complex with FLAG-tagged CcmO or CcmL by nickel-NTA affinity purification. The results showed that deletion of EP in CcmN significantly decreased the yield of CcmO or CcmL (Figure 4b,c), suggesting that CcmN EP is required for the interactions of CcmM^{NT}-CcmN with CcmL or CcmO, in agreement with previous reports.^{34,39,41} Beyond the N-terminal γ -CA domain of CcmM interacting with CcmN, the C-terminal SSUL modules of CcmM accumulate RuBisCO for the inner core assembly.³⁸ Thus the CcmM-CcmN complex functions as a central adaptor that links the shell and inner core of carboxysome.

FIGURE 3 Interfaces between CcmM^{NT} and CcmN. The interfaces of the central CcmN with (a) the lateral CcmN or (b) CcmM^{NT} in the complex. Overall structures of CcmN and CcmM^{NT} are shown as cartoon, whereas the interacting residues are shown as sticks. The polar interactions are indicated by dashed lines. (c) Comparison of the heterotrimeric CcmM^{NT}-CcmN complex with the model of trimeric CcmM^{NT} (orange, semi-transparent). The CcmM^{NT} subunit in the CcmM^{NT}-CcmN complex was aligned against subunit A of CcmM^{NT} trimer. The residues of CcmM^{NT} interacting with both CcmM^{NT} and CcmN are shown as green sticks



2.4 | The CcmM^{NT}-CcmN complex is sensitive to redox *in vitro*

One CcmN subunit contains two conserved cysteine residues, Cys49 and Cys88 (~10 Å from each other), which are located at wall C of the β -helical barrel (Figure 5a). Structural analysis revealed that two lateral CcmN subunits in an asymmetric unit of six subunits pack against each other via wall C (Figure 5a). Moreover, we unexpectedly found that Cys49 and Cys88 of one lateral CcmN have a distance of 4.1 and 5.3 Å, respectively, with their counterpart residues from the symmetric subunit. Thus upon oxidation, it is

possible to form disulfide bonds of Cys49-Cys49' and Cys88-Cys88' (residues from the symmetric subunit are labeled with a prime) between two neighboring lateral CcmN subunits (Figure 5a). To test this hypothesis, we performed the gel electrophoresis analysis of CcmN in solution upon addition of either the oxidizing agent Cu²⁺ or the reducing agent β -mercaptoethanol. The denaturing gel electrophoresis and Western blot analysis clearly showed that, the presence of 1 mM Cu²⁺ can trigger the dimerization or oligomerization of CcmN molecules, which could be reversed upon the addition of β -mercaptoethanol, indicating the formation of intermolecular disulfide bonds (Figure 5b).

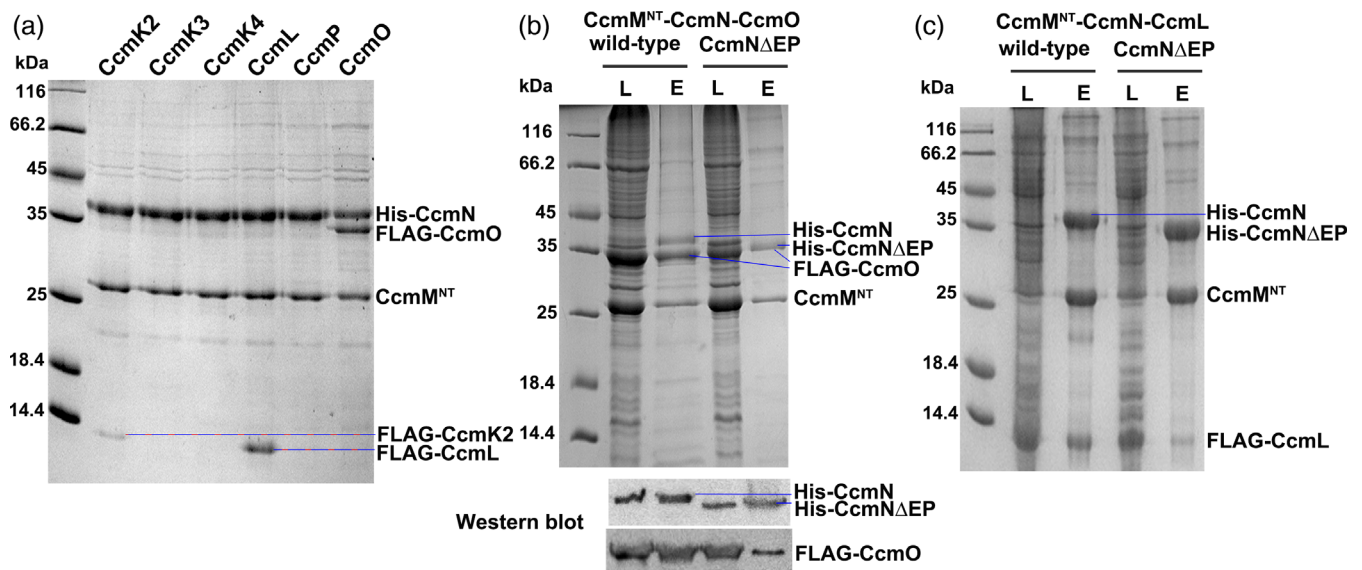


FIGURE 4 The CcmM^{NT}-CcmN complex interacts with the shell proteins CcmO and CcmL. (a) SDS-PAGE analysis of various shell proteins (CcmK2, CcmK3, CcmK4, CcmL, CcmP, CcmO) pulled down by the His-tagged SUMO-CcmN-CcmM^{NT} complex. A large amount of CcmO and CcmL proteins could be recovered as shown by SDS-PAGE. In contrast, only very little amount of CcmK2 proteins was observed in the SDS-PAGE. The other proteins were not detectable at all. SDS-PAGE (the upper panel) and Western blot (the lower panel) analysis of (b) FLAG-CcmO and (c) FLAG-CcmL pulled down by His-tagged SUMO-CcmN-CcmM^{NT} or the CcmN EP truncated version (CcmN Δ EP). The samples of cell lysates (L) and elutes (E) from nickel-NTA column were applied to the SDS-PAGE analysis. Due to the overlapped bands in the SDS-PAGE, the His-SUMO-CcmN and FLAG-CcmO were further confirmed by Western blot using anti-His and anti-FLAG antibodies, respectively

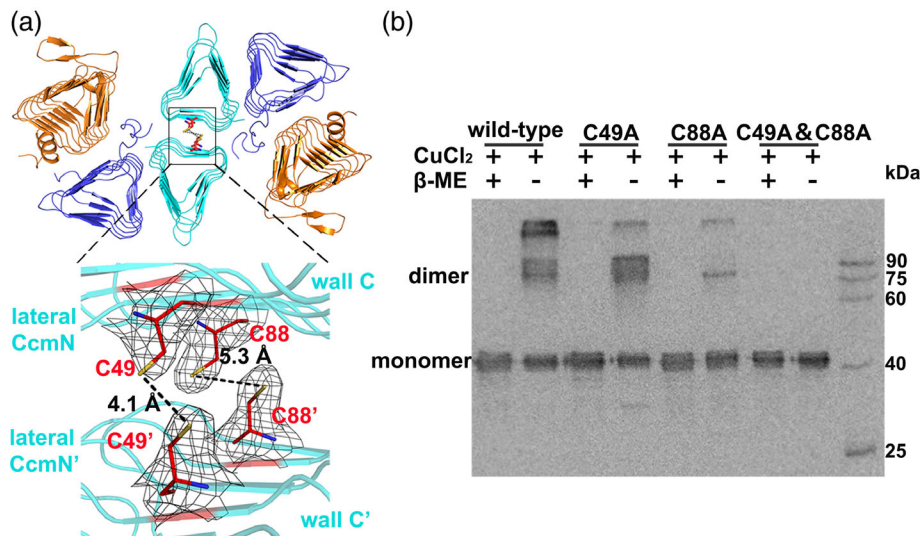


FIGURE 5 The CcmN proteins are sensitive to redox. (a) Two lateral CcmN molecules (cyan) in an asymmetric unit face against each other. As shown in the inset, the residues Cys49 and Cys88 of one lateral CcmN subunit have a distance of 4.1 and 5.3 Å, respectively, with their counterparts of the adjacent lateral CcmN subunit. The cysteine residues are shown as sticks with the electron densities shown as black mesh. (b) Western blot analysis of the disulfide bond formation of wild-type CcmN or mutants (C49A, C88A and C49A&C88A) by anti-His-tag antibody. The protein samples were incubated with 1 mM Cu²⁺ or 0.5 mM β -mercaptoethanol (β -ME), which were analyzed by SDS-PAGE and Western blot. The bands corresponding to CcmN monomer and dimer are marked on the left, whereas the standard protein markers are shown on the right

Compared to the wild-type CcmN, single mutation of either Cys49 or Cys88 to alanine drastically decreased the CcmN dimer/oligomer in the presence of Cu^{2+} (Figure 5b). Moreover, double mutations of both Cys49 and Cys88 to alanine totally abolished the disulfide bond mediated crosslinking. The results suggested that both Cys49 and Cys88 participate in the formation of intermolecular disulfide bonds, which might be involved in the regulation of carboxysome function. In fact, the inner core of β -carboxysome is found to be relatively oxidized,⁴⁵ and it has been shown that redox control is a general paradigm in carboxysome function. For example, oxidation of the conserved Cys172 inhibits the catalytic activity and stimulates the degradation of RuBisCO.⁴⁶ In contrast, the CA activity of CcaA of *S. elongatus* PCC7942 could be inhibited upon the addition of dithiothreitol.⁵ In addition, formation of a disulfide bond between the two C-terminal α -helices is required for *T. elongatus* BP-1 CcmM^{NT} to be properly structured and fully functional.¹⁷ Moreover, disulfide bond formation in the SSUL module of CcmM is required for maintaining the flexibility of RuBisCO condensate network and carboxysome function.³⁸ Altogether, in agreement with previous results, we propose that scaffolding proteins CcmM and CcmN, as well as the cargo proteins RuBisCO and CcaA, in the carboxysome are under redox control.

3 | DISCUSSION

Previous studies have investigated the interactions among β -carboxysome proteins.^{30–34,38} In *S. elongatus* PCC7942, the intact carboxysome is self-assembled by thousands of proteins from 11 different types. The most abundant proteins CcmK2 and RuBisCO constitute the major components of the shell and inner core, respectively. In addition, the scaffolding protein CcmM is also of high abundance, which bridges the shell and inner core. Quantification of β -carboxysome protein stoichiometry by real-time single-molecule fluorescence microscopy indicated that the amount of CcmN is ~10% to CcmM.⁴⁷ Thus we speculated that all CcmN molecules, due to the relatively low abundance, are very likely recruited by the N-terminal γ -CA domain of a minor portion of CcmM58, forming the CcmM-CcmN heterotrimers. Despite sharing a similar overall structure, CcmN subunit differs a lot from that of CcmM^{NT} in property of edge and wall, besides height, of the β -helical barrel, thus making it possible to form an asymmetric heterotrimer. Given the conserved interface between CcmM^{NT} and CcmN, this asymmetric CcmM-CcmN heterotrimer might represent a minimum functional unit, which acts as a

heteromeric adaptor to mediate interactions in a mortise-and-tenon pattern within carboxysome.

Our biochemical assays showed that C-terminal EP helix of CcmN contributes a great deal to the interactions with CcmO and CcmL (Figure 4b,c). Notably, a previous study indicated that CcmM mediates the interaction with the shell protein CcmK1, potentially via the helix α A of CcmM.¹⁷ Structural analysis showed that the C-terminus of CcmN in our structure stops at the same face with α A of CcmM^{NT}, further indicating EP of CcmN and α A of CcmM^{NT} are localized at the proximity to the shell proteins. A shorter β -helical barrel of CcmN, compared to that of CcmM^{NT}, gives an ideal space to accommodate the EP helix above the opening of β -helical barrel, in a pose similar to α A of CcmM. Notably, the C-terminal SSUL modules of CcmM stretch out to crosslink RuBisCO holoenzymes at the inner core of carboxysome.

The present heterotrimeric CcmM^{NT}-CcmN structure and pull-down assays, combined with the previous findings, enabled us to propose an updated model of β -carboxysome assembly. First, RuBisCO is folded and assembled into the mature form RbcL₈RbcS₈ assisted by a series of molecular chaperones, such as GroEL/ES, RbcX and Raf1.^{48–51} Afterwards, CcmM35 consisting of only SSUL modules mediates the condensation of RuBisCO, which initiates assembly of the inner core.³⁸ RuBisCO condensates expand gradually until being terminated by the full-length CcmM58 at the outermost layer of the inner core.⁵³ Notably, CcmM58 most likely exists in two forms, the homotrimer and the heterotrimeric complex with CcmN. The heterotrimeric CcmM-CcmN complexes function as adaptors that further interact with the shell proteins CcmO and CcmL, which are crucial for carboxysome formation, as deletion of *ccmO* gene resulted in severe high-CO₂-requiring phenotype (HCR) with aberrant carboxysomes, while the absence of *ccmL* led to elongated carboxysomes and the HCR phenotype.^{6,25} In addition, CcmO could recruit the major shell protein CcmK2 and probably the vertex protein CcmL,^{6,41} which might also interact with CcmK2.⁵² Thus binding of CcmO via the CcmM-CcmN complex might initiate the recruitment of other shell proteins on the inner core, and ultimately facilitate the assembly of an intact β -carboxysome.

In contrast, the majority of full-length CcmM58 proteins form homotrimers, which can also interact with the shell proteins, such as CcmK2, CcmK4, and CcmL,^{31,32,39} probably via the N-terminal γ -CA domain.³⁹ Notably, the CcmM58 homotrimers could also interact with CcaA hexamers via the N-terminal γ -CA domain, in which α A and the α A- α B loop might contribute to the interactions.²¹ However, it remains elusive on how CcmM homotrimer interacts with CcaA and shell proteins. More

investigations are needed to elucidate the fine mechanism of the intact β -carboxysome assembly in cyanobacteria.

4 | MATERIALS AND METHODS

4.1 | Cloning, plasmids, and strains

The genes encoding CcmM, CcmN, CcmK2, CcmK3, CcmK4, CcmL, CcmO, and CcmP were amplified by PCR from *S. elongatus* PCC7942 genomic DNA. CcmN was cloned into the 2ST vector, a modified vector with a ~14.2-kDa N-terminal His-SUMO tag, while other genes were cloned into the pETDuet (Novagen) expression vector using homologous recombination methods. A list of cyanobacterial strains, plasmids and protein sequences used in this study is provided in Table S1.

4.2 | Protein expression and purification

All proteins were expressed in *E. coli* strain BL21 (DE3) (Novagen) in LB medium (10 g of NaCl, 10 g of tryptone, and 5 g yeast extract per liter) containing corresponding antibiotics (30 μ g/ml kanamycin, 100 μ g/ml ampicillin, or 100 μ g/ml spectinomycin) at 37°C. When the optical density at 600 nm (OD_{600}) reached 0.8–1.0, protein expression was induced with the addition of 0.2 mM isopropyl β -D-1-thiogalactopyranoside (IPTG), followed by shaking overnight at 16°C.

The cells encoding the CcmN proteins were harvested by centrifugation (4,000 g, 4°C, 15 min), and were resuspended in buffer A of 20 mM Tris-HCl pH 7.5, 200 mM NaCl. Then the cells were lysed by 30 min of sonication. After centrifugation at 12,000 rpm for 30 min, the supernatant containing the target protein was loaded onto a nickel-NTA column (GE Healthcare) equilibrated with buffer A. And the protein was eluted using buffer A with 0.5 M imidazole and further loaded onto a Superdex 200 column (GE Healthcare) that was pre-equilibrated with buffer A. Target protein fractions were pooled and concentrated using spin columns. The protein concentration was determined using a NanoDrop (Thermo Fisher Scientific), and the purity was assessed by SDS-PAGE. The target proteins were flash-frozen in liquid nitrogen and stored at -80°C for further use. The proteins of CcmN mutants and CcmM^{NT}-CcmN complex were expressed and purified in the way similar to that of wild-type CcmN.

The *E. coli* cells expressing the complexes of CcmM^{NT}-CcmN and shell proteins were lysed and the supernatant containing the target protein was loaded

onto a nickel-NTA column equilibrated with buffer B of 20 mM Tris-HCl pH 7.5, 100 mM NaCl. The target protein was eluted with buffer B containing 0.5 M imidazole, then was dialyzed using buffer B to remove the imidazole. Finally the complex was assessed by SDS-PAGE.

4.3 | Crystallization and structure determination

Crystals of CcmM^{NT}-CcmN were grown at 16°C by sitting drop vapor diffusion with 1 μ l of 15 mg/ml protein solution and 1 μ l of reservoir solution. The crystals were grown in 0.1 M N-(2-acetamido) iminodiacetic acid, pH 6.6, 15% polyethylene glycol 8,000. X-ray diffraction data were collected at 100 K in a liquid nitrogen stream using beamline 19 U with a DECTRIS PILATUS3 6 M detector at the Shanghai Synchrotron Radiation Facility (SSRF). The diffraction data were integrated and scaled using XDS.⁵³ The crystal structure of CcmM^{NT}-CcmN was determined by molecular replacement using search models of *T. elongatus* BP-1 CcmM209 structure (PDB: 3KWC)¹⁷ and CcmN model predicted by SWISS-MODEL⁵⁴ (<http://swissmodel.expasy.org>). The structure was refined using the maximum likelihood method implemented in REFMAC5⁵⁵ as part of the CCP4i⁵⁶ program suite and rebuilt iteratively using the program Coot.⁵⁷ The final model showed well geometry and was evaluated using MolProbity⁵⁸ (<http://molprobity.biochem.duke.edu>). All interface areas were calculated by PDBsum,⁵⁹ All structure figures were prepared with PyMOL (<https://pymol.org/2/>). A list of the parameters of data collection, processing, structure determination and refinement is provided in Table S2.

4.4 | Size exclusion chromatography with multi-angle light scattering

Analytical SEC was performed using an AKTA Pure system (GE Healthcare) with a Superdex 200 10/300 GL column (GE Healthcare). The system was coupled on-line to an eight-angle MALS detector (DAWN HELEOS II, Wyatt Technology) and a differential refractometer (Optilab T-rEX, Wyatt Technology). The molecular mass of CcmM^{NT} trimer or CcmM^{NT}-CcmN complex in solution was determined using ASTRA 7.0.1 software.

4.5 | Redox assays of CcmN

The CcmN proteins or mutants were incubated in buffer A with 1 mM CuCl₂ on ice for 30 min. Each sample was

equally divided into two parts, with or without 0.5 mM β -mercaptoethanol. Samples were boiled for 10 min, then applied to SDS-PAGE analysis to detect the formation of disulfide bonds.

4.6 | Western blotting

The protein bands in SDS-PAGE were transferred to PVDF membranes activated by methanol. Experiments were performed at 250 mA for 2 hr at 4°C in the transfer buffer (25 mM Tris-HCl, 192 mM glycine, 20% [v:v] ethanol). The blots were blocked with 5% skimmed milk overnight at 4°C. The primary mouse anti-His or anti-FLAG antiserum (Proteintech) were diluted 1:2,500, while the second rabbit anti-mouse IgG (Proteintech) was diluted 1:5,000 in the TBST buffer (100 mM Tris-HCl pH 7.5, 150 mM NaCl, 0.1% Tween). Between every step, the PVDF membranes were washed five times with TBST buffer. Finally, the blots were developed using Amersham ECL Western blotting detection reagents (GE healthcare) and imaged using ImageQuant LAS 4000.

ACKNOWLEDGMENTS

We thank the staff at the Shanghai Synchrotron Radiation Facility (SSRF) for technical assistance. This work is supported by the Strategic Priority Research Program of the Chinese Academy of Sciences (<http://www.cas.cn>; grant numbers XDA24020302 and XDB37020301), National Natural Science Foundation of China (www.nsf.gov.cn; grant numbers 31630001 and 31621002) and the Fundamental Research Funds for the Central Universities. Y.-L.J. thanks the Youth Innovation Promotion Association of Chinese Academy of Sciences for their support.

CONFLICT OF INTEREST

The authors declare no competing interests.

AUTHOR CONTRIBUTIONS

Hui Sun: Data curation; formal analysis; investigation; validation; writing-original draft. **Ning Cui:** Data curation; formal analysis. **Shu-Jing Han:** Data curation; methodology. **Zhi-Peng Chen:** Data curation; methodology. **Ling-Yun Xia:** Data curation; methodology. **Yuxing Chen:** Conceptualization; supervision. **Yong-Liang Jiang:** Conceptualization; data curation; formal analysis; funding acquisition; supervision; writing-original draft; writing-review & editing. **Cong-Zhao Zhou:** Conceptualization; funding acquisition; writing-review & editing.

DATA AVAILABILITY STATEMENT

Crystal structure of CcmM^{NT} in complex with CcmN has been deposited at PDB under the accession code of 7D6C.

ORCID

Cong-Zhao Zhou  <https://orcid.org/0000-0002-6881-7151>

REFERENCES

1. Badger MR, Price GD. CO₂ concentrating mechanisms in cyanobacteria: Molecular components, their diversity and evolution. *J Exp Bot.* 2003;54:609–622.
2. Price GD. Inorganic carbon transporters of the cyanobacterial CO₂ concentrating mechanism. *Photosynth Res.* 2011;109:47–57.
3. Shively JM, Ball F, Brown DH, Saunders RE. Functional organelles in prokaryotes: Polyhedral inclusions (carboxysomes) of *Thiobacillus neapolitanus*. *Science.* 1973;182:584–586.
4. Cannon GC, Shively JM. Characterization of a homogenous preparation of carboxysomes from *Thiobacillus neapolitanus*. *Arch Microbiol.* 1983;134:52–59.
5. Price GD, Coleman JR, Badger MR. Association of carbonic anhydrase activity with carboxysomes isolated from the cyanobacterium *Synechococcus* PCC7942. *Plant Physiol.* 1992;100:784–793.
6. Rae BD, Long BM, Badger MR, Price GD. Structural determinants of the outer shell of beta-carboxysomes in *Synechococcus elongatus* PCC 7942: Roles for CcmK2, K3-K4, CcmO, and CcmL. *PLoS One.* 2012;7:e43871.
7. Kinney JN, Axen SD, Kerfeld CA. Comparative analysis of carboxysome shell proteins. *Photosynth Res.* 2011;109:21–32.
8. Price GD, Badger MR. Evidence for the role of carboxysomes in the cyanobacterial CO₂-concentrating mechanism. *Can J Bot.* 1991;69:963–973.
9. Schmid MF, Paredes AM, Khant HA, et al. Structure of *Halothiobacillus neapolitanus* carboxysomes by cryo-electron tomography. *J Mol Biol.* 2006;364:526–535.
10. Rae BD, Long BM, Badger MR, Price GD. Functions, compositions, and evolution of the two types of carboxysomes: Polyhedral microcompartments that facilitate CO₂ fixation in cyanobacteria and some proteobacteria. *Microbiol Mol Biol Rev.* 2013;77:357–379.
11. Kerfeld CA, Melnicki MR. Assembly, function and evolution of cyanobacterial carboxysomes. *Curr Opin Plant Biol.* 2016;31:66–75.
12. Newman J, Branden CI, Jones TA. Structure determination and refinement of ribulose 1,5-bisphosphate carboxylase/oxygenase from *Synechococcus* PCC6301. *Acta Crystallogr D Biol Crystallogr.* 1993;49:548–560.
13. Kerfeld CA, Sawaya MR, Tanaka S, et al. Protein structures forming the shell of primitive bacterial organelles. *Science.* 2005;309:936–938.
14. Tsai Y, Sawaya MR, Cannon GC, et al. Structural analysis of CsoS1A and the protein shell of the *Halothiobacillus neapolitanus* carboxysome. *PLoS Biol.* 2007;5:e144.
15. Tanaka S, Kerfeld CA, Sawaya MR, et al. Atomic-level models of the bacterial carboxysome shell. *Science.* 2008;319:1083–1086.

16. Klein MG, Zwart P, Bagby SC, et al. Identification and structural analysis of a novel carboxysome shell protein with implications for metabolite transport. *J Mol Biol.* 2009;392:319–333.
17. Peña KL, Castel SE, de Araujo C, Espie GS, Kimber MS. Structural basis of the oxidative activation of the carboxysomal γ -carbonic anhydrase, CcmM. *Proc Natl Acad Sci U S A.* 2010;107:2455–2460.
18. Samborska B, Kimber MS. A dodecameric CcmK2 structure suggests beta-carboxysomal shell facets have a double-layered organization. *Structure.* 2012;20:1353–1362.
19. Cai F, Sutter M, Cameron JC, Stanley DN, Kinney JN, Kerfeld CA. The structure of CcmP, a tandem bacterial microcompartment domain protein from the beta-carboxysome, forms a subcompartment within a microcompartment. *J Biol Chem.* 2013;288:16055–16063.
20. Cai F, Sutter M, Bernstein SL, Kinney JN, Kerfeld CA. Engineering bacterial microcompartment shells: Chimeric shell proteins and chimeric carboxysome shells. *ACS Synth Biol.* 2015;4:444–453.
21. McGurn LD, Moazami-Goudarzi M, White SA, et al. The structure, kinetics and interactions of the beta-carboxysomal β -carbonic anhydrase, CcaA. *Biochem J.* 2016;473:4559–4572.
22. Ryan P, Forrester TJB, Wroblewski C, et al. The small RbcS-like domains of the beta-carboxysome structural protein CcmM bind RubisCO at a site distinct from that binding the RbcS subunit. *J Biol Chem.* 2019;294:2593–2603.
23. Badger MR, Hanson D, Price GD. Evolution and diversity of CO₂ concentrating mechanisms in cyanobacteria. *Funct Plant Biol.* 2002;29(3):161–173.
24. Iancu CV, Morris DM, Dou Z, Heinhorst S, Cannon GC, Jensen GJ. Organization, structure, and assembly of alpha-carboxysomes determined by electron cryotomography of intact cells. *J Mol Biol.* 2010;396:105–117.
25. Cameron JC, Wilson SC, Bernstein SL, Kerfeld CA. Biogenesis of a bacterial organelle: The carboxysome assembly pathway. *Cell.* 2013;155:1131–1140.
26. Cai F, Dou Z, Bernstein SL, et al. Advances in understanding carboxysome assembly in *Prochlorococcus* and *Synechococcus* implicate CsoS2 as a critical component. *Life (Basel).* 2015;5:1141–1171.
27. Chaijarasphong T, Nichols RJ, Kortright KE, et al. Programmed ribosomal frameshifting mediates expression of the α -carboxysome. *J Mol Biol.* 2016;428:153–164.
28. Liu Y, He X, Lim W, et al. Deciphering molecular details in the assembly of α -type carboxysome. *Sci Rep.* 2018;8:15062.
29. Oltrogge LM, Chaijarasphong T, Chen AW, Bolin ER, Marqusee S, Savage DF. Multivalent interactions between CsoS2 and Rubisco mediate α -carboxysome formation. *Nat Struct Mol Biol.* 2020;27:281–287.
30. Long BM, Badger MR, Whitney SM, Price GD. Analysis of carboxysomes from *Synechococcus* PCC7942 reveals multiple Rubisco complexes with carboxysomal proteins CcmM and CcaA. *J Biol Chem.* 2007;282:29323–29335.
31. Cot SS, So AK, Espie GS. A multiprotein bicarbonate dehydration complex essential to carboxysome function in cyanobacteria. *J Bacteriol.* 2008;190:936–945.
32. Long BM, Tucker L, Badger MR, Price GD. Functional cyanobacterial beta-carboxysomes have an absolute requirement for both long and short forms of the CcmM protein. *Plant Physiol.* 2010;153:285–293.
33. Long BM, Rae BD, Badger MR, Price GD. Over-expression of the beta-carboxysomal CcmM protein in *Synechococcus* PCC7942 reveals a tight co-regulation of carboxysomal carbonic anhydrase (CcaA) and M58 content. *Photosynth Res.* 2011;109:33–45.
34. Kinney JN, Salmeen A, Cai F, Kerfeld CA. Elucidating essential role of conserved carboxysomal protein CcmN reveals common feature of bacterial microcompartment assembly. *J Biol Chem.* 2012;287:17729–17736.
35. Faulkner M, Rodriguez-Ramos J, Dykes GF, et al. Direct characterization of the native structure and mechanics of cyanobacterial carboxysomes. *Nanoscale.* 2017;9:10662–10673.
36. Price GD, Howitt SM, Harrison K, Badger MR. Analysis of a genomic DNA region from the cyanobacterium *Synechococcus* sp. strain PCC7942 involved in carboxysome assembly and function. *J Bacteriol.* 1993;175:2871–2879.
37. Ludwig M, Sültemeyer D, Price GD. Isolation of *ccmKLMN* genes from the marine cyanobacterium *Synechococcus* sp. PCC 7002 and evidence that CcmM is essential for carboxysome assembly. *J Phycol.* 2000;36:1109–1118.
38. Wang H, Yan X, Aigner H, et al. Rubisco condensate formation by CcmM in β -carboxysome biogenesis. *Nature.* 2019;566:131–135.
39. Cai F, Bernstein SL, Wilson SC, Kerfeld CA. Production and characterization of synthetic carboxysome shells with incorporated luminal proteins. *Plant Physiol.* 2016;170:1868–1877.
40. Aussignargues C, Paasch BC, Gonzalez-Esquer R, Erbilgin O, Kerfeld CA. Bacterial microcompartment assembly: The key role of encapsulation peptides. *Commun Integr Biol.* 2015;8:e1039755.
41. Lin MT, Occhialini A, Andralojc PJ, et al. β -Carboxysomal proteins assemble into highly organized structures in *Nicotiana* chloroplasts. *Plant J.* 2014;79:1–12.
42. Fan CG, Bobik TA. The N-terminal region of the medium subunit (PduD) packages adenosylcobalamin-dependent diol dehydratase (PduCDE) into the Pdu microcompartment. *J Bacteriol.* 2011;193:5623–5628.
43. Jakobson CM, Kim EY, Slininger MF, Chien A, Tullman-Ercek D. Localization of proteins to the 1,2-propanediol utilization microcompartment by non-native signal sequences is mediated by a common hydrophobic motif. *J Biol Chem.* 2015;290:24519–24533.
44. So AKC, Espie GS. Cyanobacterial carbonic anhydrases. *Can J Bot.* 2005;83:721–734.
45. Chen AH, Robinson-Mosher A, Savage DF, Silver PA, Polka JK. The bacterial carbon-fixing organelle is formed by Shell envelopment of preassembled cargo. *PLoS One.* 2013;8(9):e76127.
46. Marcus Y, Altman-Gueta H, Finkler A, Gurevitz M. Dual role of cysteine 172 in redox regulation of ribulose 1,5-bisphosphate carboxylase/oxygenase activity and degradation. *J Bacteriol.* 2003;185:1509–1517.
47. Sun Y, Wollman AJM, Huang F, Leake MC, Liu LN. Single-organelle quantification reveals stoichiometric and structural variability of carboxysomes dependent on the environment. *Plant Cell.* 2019;31:1648–1664.

48. Saschenbrecker S, Bracher A, Rao KV, Rao BV, Hartl FU, Hayer-Hartl M. Structure and function of RbcX, an assembly chaperone for hexadecameric Rubisco. *Cell*. 2007;129:1189–1200.
49. Hayer-Hartl M, Bracher A, Hartl FU. The GroEL-GroES chaperonin machine: A nano-cage for protein folding. *Trends Biochem Sci*. 2016;41:62–76.
50. Huang F, Vasieva O, Sun Y, et al. Roles of RbcX in carboxysome biosynthesis in the cyanobacterium *Synechococcus elongatus* PCC7942. *Plant Physiol*. 2019;179:184–194.
51. Xia LY, Jiang YL, Kong WW, et al. Molecular basis for the assembly of RuBisCO assisted by the chaperone Raf1. *Nat Plants*. 2020;6:708–717.
52. Sutter M, Laughlin TG, Sloan NB, Serwas D, Davies KM, Kerfeld CA. Structure of a synthetic beta-Carboxysome shell. *Plant Physiol*. 2019;181:1050–1058.
53. Kabsch W. XDS. *Acta Crystallogr D Biol Crystallogr*. 2010;66:125–132.
54. Schwede T, Kopp J, Guex N, Peitsch MC. SWISS-MODEL: An automated protein homology-modeling server. *Nucleic Acids Res*. 2003;31:3381–3385.
55. Murshudov GN, Vagin AA, Dodson EJ. Refinement of macromolecular structures by the maximum-likelihood method. *Acta Crystallogr D Biol Crystallogr*. 1997;53:240–255.
56. Winn MD, Ballard CC, Cowtan KD, et al. Overview of the CCP4 suite and current developments. *Acta Crystallogr D Biol Crystallogr*. 2011;67:235–242.
57. Emsley P, Cowtan K. Coot: Model-building tools for molecular graphics. *Acta Crystallogr D Biol Crystallogr*. 2004;60:2126–2132.
58. Davis IW, Leaver-Fay A, Chen VB, et al. MolProbity: All-atom contacts and structure validation for proteins and nucleic acids. *Nucleic Acids Res*. 2007;35:W375–383.
59. Laskowski RA. PDBsum: Summaries and analyses of PDB structures. *Nucleic Acids Res*. 2001;29:221–222.

SUPPORTING INFORMATION

Additional supporting information may be found online in the Supporting Information section at the end of this article.

How to cite this article: Sun H, Cui N, Han S-J, et al. Complex structure reveals CcmM and CcmN form a heterotrimeric adaptor in β -carboxysome. *Protein Science*. 2021;1–11. <https://doi.org/10.1002/pro.4090>